Dimerization-Induced Activation of Soluble Insulin/IGF-1 Receptor Kinases: An Alternative Mechanism of Activation†

Kristin Baer,‡ Hadi Al-Hasani,‡ Susan Parvaresch, Theresa Corona, Arne Rufer, Volker Nölle, Eva Bergschneider, and Helmut W. Klein*

Institute of Biochemistry, University of Cologne, Otto-Fischer-Strasse 12-14, 50674 Cologne, Germany

Received July 18, 2001; Revised Manuscript Received October 1, 2001

ABSTRACT: To study the role of kinase dimerization in the activation of the insulin receptor (IR) and the insulin-like growth factor receptor-1 (IGF-1R), we have cloned, expressed, and purified monomeric and dimeric forms of the corresponding soluble kinase domains via the baculovirus expression system. Dimerization of the kinases was achieved by fusion of the kinase domains to the homodimeric glutathione *S*-transferase (GST). Kinetic analyses revealed that kinase dimerization results in substantial increases (10−100-fold) in the phosphotransferase activity in both the auto- and substrate phosphorylation reactions. Furthermore, kinase dimerization rendered the autophosphorylation reaction concentration-independent. However, whereas dimerization was required for the rapid autophosphorylation of the kinases, it was not essential for the enhanced kinase activity in substrate phosphorylation reactions. Comparison of HPLC-phosphopeptide maps of the monomeric and dimeric kinases revealed that dimerization leads to an increased phosphorylation of the regulatory activation loop of the kinases, strongly suggesting that bis- and trisphosphorylation of the activation loop are mediated by transphosphorylation within the kinase dimers. Most strikingly, limited proteolysis revealed that GST-mediated dimerization by itself had a major impact on the conformation of the activation loop by stabilizing a conformation that corresponds to the active, phosphorylated form of the kinase. Thus, in analogy to the insulin/IGF-1-ligated holoreceptors, the dimeric GST-kinases are primed to rapid autophosphorylation by an increase in the local concentration of both phosphoryl donor and phosphoryl acceptor sites and by a dimerization-induced conformational change of the activation loop that leads to an efficient transphosphorylation of the regulatory tyrosine residues.

Ligand-induced activation of growth hormone receptors such as epidermal growth factor receptor (EGFR) and platelet-derived growth factor receptor (PDGFR) involves receptor dimerization and subsequent transautophosphorylation of their cytosolic protein kinase domains, respectively (*1*). However, the members of the insulin receptor family (IR,[1] IGF-1R) are different from most other receptor kinases by being in a dimerized state even in the absence of their ligands. Several lines of evidence suggest that insulin/IGF1 binding to the extracellular ligand binding domains induces conformational changes in the receptor (*2*−*4*). These changes are believed to result in a spatial rearrangement of the two intracellular kinase subunits, leading to an efficient transphosphorylation of three regulatory tyrosine residues within the activation loop of the enzyme and subsequent kinase activation (*5*). According to the "cis-inhibition/trans-activation model" (*6*), it has been proposed that the nonphosphorylated activation loop of the insulin receptor kinase has an autoinhibitory function (referred to as cis-inhibition) by interfering with access of metal-ATP to the active site. Tyrosine autophosphorylation of the activation loop (presumably in trans) causes a relief of this inhibition, thereby enabling metal-ATP binding and subsequent activation of the kinase (*6*).

The soluble monomeric insulin receptor kinase domain (IRKD) has been widely used as a model enzyme to study the molecular mechanism of IR kinase activation (*7*−*12*). However, due to its low intrinsic activity, the monomeric IRKD has been proposed as a model for the nonactivated (nonligated) insulin receptor rather than for the insulin-stimulated holoreceptor (*9*). Nevertheless, autophosphorylation of monomeric IRKD at very high concentrations (>10 μM) and extended reaction times (60 min) has been described to fully activate the enzyme where the activity persisted even after dilution of the phosphorylated enzyme (*13*, *14*). Likewise, poly-L-lysine-mediated IRKD oligomerization has been shown to dramatically increase the catalytic activity of the soluble receptor kinase (*8*, *15*−*17*). Thus, one might speculate that an increase in the local concentration of kinase molecules leads to an increased rate of transphosphorylation, resulting in a more efficient and rapid phosphorylation of the key residues in the activation loop. Nevertheless, the IRKD model does not reflect the conditions in the native holoreceptor where the two kinase containing β subunits are juxtaposed in the $(\alpha\beta)_2$ dimer. Although it has been shown that intermolecular phosphorylation between dimeric insulin

† This work was supported in part by the Deutsche Forschungsgemeinschaft (SFB 351/C1).

* To whom correspondence should be addressed. Tel.: +49 221 470-3208. Fax: +49 221 470-5066. E-mail: h-w.klein@uni-koeln.de.

‡ These authors contributed equally to this work.

[1] Abbreviations used: GST, glutathione-*S*-transferase; IGF-1R, insulin-like growth factor-1 receptor; IGFKD, soluble insulin-like growth factor-1 receptor kinase domain; IR, insulin receptor; IRKD, soluble insulin receptor kinase domain; IRS1, insulin receptor substrate-1; MALDI-TOF, matrix-assisted laser desorption and ionization time-of-flight mass spectrometry; p85, 85 kDa regulatory subunit of phosphatidylinositol (PI) 3-kinase; SH2, src-homology domain 2; *Sf9*, *Spodoptera frugiperda*.

10.1021/bi015588g CCC: $20.00
Published on Web 11/02/2001

receptors does not increase the kinase activity of the IR (*18*), there is little information about the contribution of the dimeric structure of the IR to the activation of the kinase. Several reports have suggested that the ligand-induced conformational changes in tyrosine kinase receptors cannot be attained simply by the introduction of a dimerizing sequence into the protein (reviewed in ref *19*). For instance, both the insulin and the *neu* (ErbB-2) receptors lost their activity when their transmembrane domains were replaced with that of the strongly dimerizing transmembrane domain of glycophorin A (*20*, *21*). Thus, whereas kinase dimerization appears to be required for kinase activation, it remains unclear whether dimerization alone is sufficient for kinase activation. To study the role of dimerization in IR/IGF-1R receptor kinase activation, we have constructed homodimeric soluble kinase domains derived from the IR and the IGF-1R, respectively. Dimerization was achieved by expression of glutathione *S*-transferase (GST) fusion proteins that form stable noncovalent dimers during protein synthesis (*22*, *23*). Our results show that dimerization of the receptor kinases greatly enhances the catalytic activity of the enzymes.

EXPERIMENTAL PROCEDURES

Materials. The plasmid coding for the N-terminal SH2 domain of the 85 kDa regulatory subunit of phosphatidylinositol (PI) 3-kinase (p85) was a generous gift from Steven E. Shoelson (Harvard Medical School, Boston, MA). [γ^{32}P]-ATP (6000 Ci/mmol) was obtained from Amersham Pharmacia Biotech. Restriction endonucleases were from MBI Fermentas and Roche. *Pfu* polymerase was from Stratagene; ADP and ATP were from Roche. Thrombin was from PharminGen. Cell culture reagents were from Life Technologies Inc.; poly-L-lysine (M_r 15 000−30 000) was from Serva. For HPLC phosphopeptide maps, trypsin (sequencing grade) from Merck was used. Other reagents were obtained from common commercial sources.

Construction of Soluble Receptor Kinases. The construction of IRKD and IGFKD was previously described (*11*, *24*). *GST-IRKD*: A cDNA fragment corresponding to R941-S1343 of the human IR was generated by PCR to contain *Bam*HI and *Eco*RI restriction sites using *Pfu* polymerase (Stratagene). The primers were (sense strand) 5′-GGG ATC CTA TAG GAT CCA GAA AGA GGC AGC CAG ATG G-3′ and (anti-sense strand) 5′-CGC CAC GGT AGG AAT TCT TAG GAA GGA TTG GACC-3′. The resulting *Bam*HI/*Eco*RI fragment was subcloned into the baculovirus transfer vector pAcG2T (PharminGen). *GST-IGFK*: A *Bam*HI restriction site was introduced into the cDNA by site-directed mutagenesis by using the QuikChange site-directed mutagenesis kit (Stratagene). The primers (mismatches underlined) were (sense strand) 5′-TTA TTT CTC TTT CTG GAT CCT ATA GAA TTC ACT GGCC-3′ and (anti-sense strand) 5′-CAG TGA ATT CTA TAG GAT CCA GAA AGA GAA ATA ACA GC-3′. A *Bam*HI fragment corresponding to R930-C1337 was subcloned into the baculovirus transfer vector pAcG2T (PharminGen). The integrity of all constructs was verified by automated sequencing. Cotransfection of *Spodoptera frugiperda* (*Sf9*) cells and isolation of recombinant baculoviruses were performed as described (*11*).

Construction of IRS1-p10. A fragment of the human IRS-1 (*25*) corresponding to R657-L760 was PCR-amplified to contain *Bam*HI and *Eco*RI restriction sites using *Pfu* polymerase (Stratagene). The primers were (sense strand) 5′-GCC GGA TCC AGA GAG TGG ACC CCA ATG GC-3′ and (anti-sense strand) 5′-GAG GAA TTC GGC TTG TGC TGG GGG TCC TCA GG-3′. The resulting *Bam*HI/*Eco*RI fragment was subcloned into pGEX3X (Amersham Pharmacia Biotech). The integrity of the construct was verified by automated sequencing.

Purification of Recombinant Proteins. Purification of IRKD from baculovirus-infected *Sf9* cells was accomplished by sequential chromatography using ResourceQ and Phenyl-Sepharose (Amersham Pharmacia Biotech) as described previously (*11*). *Sf9* cells containing GST-tagged kinases were lysed in 20 mM Tris/HCl pH 7.5, 250 mM Sucrose, 0.1% Triton X-100, and 1 mM DTT by mild sonication. Cleared lysates were used for affinity chromatography with glutathione sepharose (Amersham Pharmacia Biotech) according to the manufacturer's instructions. The resulting eluates were washed with 50 mM Tris/HCl pH 7.5, 1 mM DTT, concentrated by ultrafiltration, and stored at −80 °C. To obtain soluble monomeric kinases by enzymatic cleavage, GST-kinases were incubated with thrombin at 0.1−0.2 U/100 μg protein for 30 min at room temperature. The samples were passed over a ResourceQ anion exchange column, and the fractions containing the monomeric kinases were pooled and concentrated by ultrafiltration. Expression and purification of GST-tagged IRS1-p10 from *E. coli* were performed as described (*26*).

Phosphorylation Reactions. All phosphorylation reactions were carried out at room temperature (22 °C).

(i) *Autophosphorylation Reactions.* The reaction mixtures contained 50 mM Tris/HCl, pH 7.5, 5 mM $MgCl_2$, 5 mM $MnCl_2$, and 250 μM [γ^{32}P]ATP (GST-kinases: additionally 1 mM DTT). Unless indicated otherwise, the kinase concentration was 0.5−1 μM. Where indicated, poly-L-lysine (average M_r 22 500) was added in equimolar amounts to the kinases. The phosphorylated proteins were separated by sodium dodecyl sulfate−polyacrylamide gel electrophoresis (SDS−PAGE), localized by autoradiography, and the radioactivity of the excised bands was determined by measurement of the Cerenkov radiation in a Beckman scintillation counter.

(ii) *Substrate Phosphorylation Reactions.* Both GST-IRKD and IRKD were prephosphorylated for 3 min at concentrations of 1 μM. Substrate phosphorylation reactions were carried out at a kinase concentration of 0.3 μM in 50 mM Tris/HCl, pH 7.5, 250 μM [γ^{32}P]ATP, 5 mM $MgCl_2$, 5 mM $MnCl_2$, 0.1 mM DTT, and 0.1% (w/v) BSA. After 3 min of reaction time, phosphorylation reactions were quenched by adding EDTA. Phosphate incorporation into IRS1-p10 was determined after SDS−PAGE and Cerenkov-counting of the excised gel bands. Substrate phosphorylation reactions of poly(Glu_4:Tyr) were carried out using the phosphocellulose paper assay (*27*).

HPLC-Phosphopeptide Mapping. (i) *Generation of Tryptic Phosphopeptides*. The autophosphorylated soluble kinases were eluted after SDS−PAGE as described previously (*11*). The recovery of [^{32}P]-labeled peptides typically exceeded 90%.

(ii) *Separation of Tryptic Phosphopeptides*. Phosphopeptides were separated on a Beckman Gold HPLC system using an anion exchange column (Macherey-Nagel, Nucleogel SAX-1000-8/46) as described previously (*11*). Monitoring

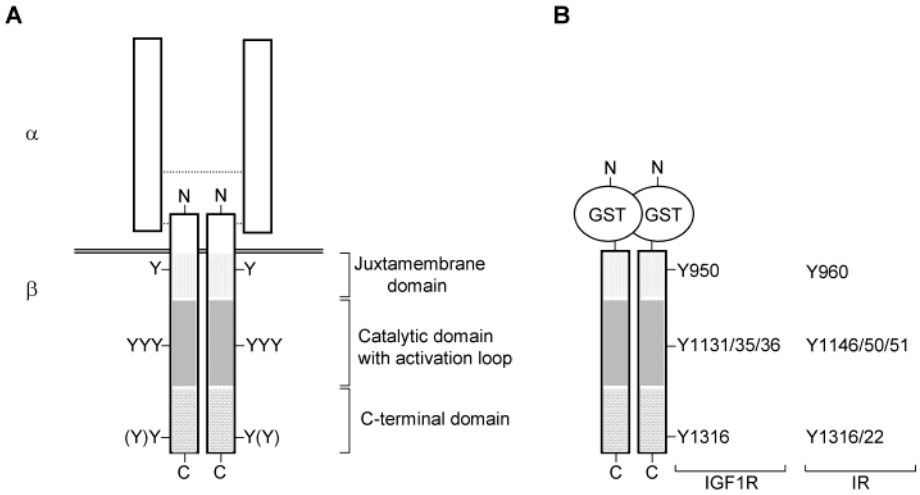

FIGURE 1: Topology of the insulin receptor/insulin-like growth factor receptor. (A) Schematic domain organization of the dimeric $(\alpha\beta)_2$ holoreceptors. In their cytosolic domains, the insulin receptor and the IGF-1 receptor show high sequence homology (68% identity, 78% similarity). Indicated are the three subdomains of the cytosolic β subunits (juxtamembrane domain, catalytic domain (containing the activation loop) and the C-terminal domain) and the positions of tyrosine autophosphorylation sites. (B) Schematic representation of the dimeric GST-tagged kinases. Indicated are the tyrosine autophosphorylation sites of the insulin receptor (Y960, Y1146, Y1150, Y1151, Y1316, and Y1322) and the IGF-1 receptor (Y950, Y1131, Y1135, Y1136, and Y1316).

of the eluted radioactivity was achieved by using a HPLC radiometer 505TR from Packard with a 0.5 mL Cerenkov flow-through cell.

Molecular Mass Analysis. (i) *Native Gradient PAGE*. Native gel electrophoresis was performed in 20 cm long 3.5−25% polyacrylamide gels at 10 mA for 19 h at 4 °C. Molecular mass standard proteins were from Amersham Pharmacia Biotech.

(ii) *Mass Spectrometry.* Matrix-assisted laser desorption and ionization time-of-flight mass spectrometry (MALDI-TOF) was performed on a Bruker reflex III instrument (Bruker Daltonik GmbH, Bremen, Germany). Samples of ~1 nmol were cocrystallized with sinapinic acid as the matrix. Individual spectra were obtained at each step by collecting 210 laser shots. Spectra were externally calibrated using bovine serum albumin as the standard.

Limited Proteolysis. GST-IRKD (10 μM) and IRKD (8 μM) were diluted in reaction buffer (50 mM Tris/acetate pH 7.0, 1 mM DTT, 2 mM $CaCl_2$) with or without 20 mM Mg-acetate/10 mM adenine nucleotides and equilibrated at room temperature for 3 min. Trypsin (sequencing grade; Merck) was then added as indicated, and the reaction was carried out at room temperature for indicated times. The reactions were stopped by adding SDS sample buffer (*28*). Cleavage products were resolved by 15% SDS−PAGE. The gels were then stained overnight in a colloidal suspension of Coomassie Blue (*29*) and destained in H_2O.

Far-Western Analysis. Purified GST-IRKD was autophosphorylated for 30 min in the presence of [γ^{32}P]ATP and then repurified again by affinity chromatography on gluthatione sepharose. Samples containing GST-p85/SH2 or GST were subjected to SDS−PAGE and transferred to PVDF membranes, which were then blocked with 5% (w/v) skim milk in PBS, 0.1% Tween-20 for 1 h at room temperature. The membrane with the immobilized proteins was then incubated for 2 h at room temperature with the [^{32}P]-labeled GST-kinase. After several washes with PBS, the membrane was exposed to a Phospho-Imager screen (Bio-Rad Imaging System).

Other Procedures. *Spodoptera frugiperda* (*Sf9*) cells were maintained as described (*11*). Protein concentrations were determined by a modified method of Bradford (*30*). SDS−PAGE was performed according to Laemmli (*28*). Protein staining after SDS−PAGE was carried out by a modified colloidal Coomassie stain (*29*).

RESULTS

Construction and Purification of Monomeric and Dimeric Soluble Receptor Kinases. The entire cytosolic domains of the insulin receptor (IRKD) and the insulin-like growth factor-1 receptor (IGFKD) were expressed as GST fusion proteins in insect cells and purified to homogeneity by affinity chromatography (Figure 1; see Experimental Procedures). In addition, a nontagged IRKD was expressed and purified by sequential chromatography as previously described (*11*). Figure 2 illustrates the course of purification for the enzymes. All of the constructs showed similar expression levels (3−5% of total protein) and similar yields (1−2 mg purified protein per 2×10^8 cells). Nontagged IGFKD was obtained by removal of the GST tag from affinity purified GST-IGFKD by thrombin-cleavage and subsequent anion exchange chromatography (Figure 2; see Experimental Procedures).

The GST-Tagged Kinases Are Constitutive Dimers. As shown in Figure 2, both GST-tagged kinases, GST-IRKD and GST-IGFKD, showed an apparent M_r of ~76 000 in SDS−PAGE, whereas both nontagged enzymes, IRKD and IGFKD, migrated according to an M_r of ~50 000, respectively. Thus, under denaturating conditions, both observed apparent M_r's closely reflect their predicted values of 46 000 for the nontagged and 72 000 for the GST-tagged kinases, respectively. As expected, in nondenaturating PAGE, GST-IRKD showed an apparent M_r of ~143 000 , whereas the apparent M_r of the nontagged IRKD was 49 000 (Figure 3A; see Experimental Procedures), indicating dimerization of the GST-tagged kinase. Similar M_r's were obtained by gel permeation chromatography (data not shown). Likewise, as indicated in Figure 3B, MALDI-TOF mass spectroscopy

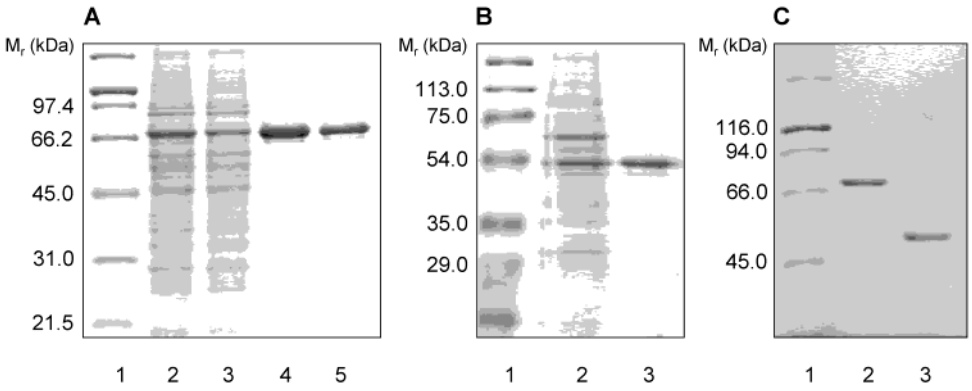

FIGURE 2: Purification of soluble kinases. Samples were resolved by SDS−PAGE and visualized by Coomassie staining. (A) Purification of GST-tagged kinases: 1, marker; 2 and 3, crude cell lysates of *Sf*9 cells expressing GST-IRKD and GST-IGFKD; 4 and 5, affinity purified GST-IRKD and GST-IGFKD. (B) Purification of soluble monomeric IRKD by sequential chromatography: 1, marker; 2, crude cell lysate of *Sf*9 cells expressing IRKD; 3, purified IRKD. (C) Purification of soluble monomeric IGFKD: 1, marker; 2, affinity purified GST-IGFKD; 3, purified IGFKD after thrombin-cleavage and anion exchange chromatography (see Experimental Procedures).

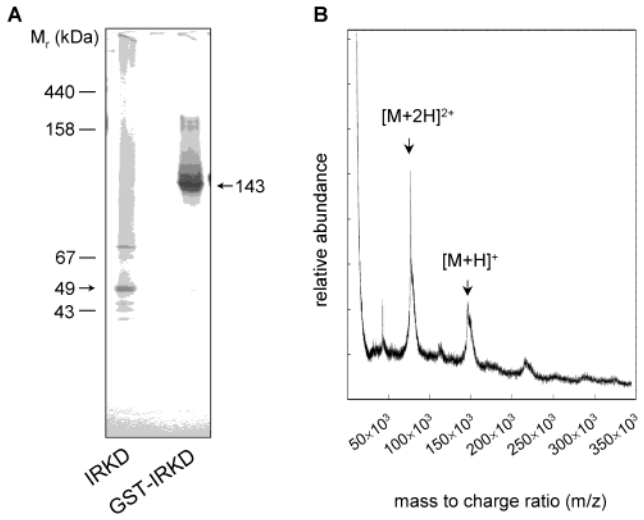

FIGURE 3: The GST-tagged kinases are constitutive dimers. (A) Samples containing IRKD and GST-IRKD were separated on a 3.5−25% native gradient gel for 19 h at 4 °C and stained with Coomassie Blue. Markers were ovalbumin (43 kDa), bovine serum albumin (67 kDa), aldolase (158 kDa), and ferritin (440 kDa). Arrows indicate the positions of IRKD (49 kDa) and GST-IRKD (143 kDa). (B) MALDI spectrum of GST-IGFKD. Indicated by arrows are the peaks for the singly charged molecular ions, $[M + H]^+$ at *m*/*z* 144 114, and the doubly charged ions, $[M + 2H]^{2+}$ at *m*/*z* 71 579.

revealed two peaks; one peak corresponds to a M_r of 144 100 for the singly charged ion, consistent with the presence of GST-IGFKD dimers. The second peak (M_r of 71 600) corresponds to the doubly charged dimeric enzyme. Thus, as expected, whereas expression of the soluble cytosolic domains of the insulin receptor and the insulin-like growth factor-1 receptor yields monomeric enzymes, the corresponding GST fusion proteins are constitutive dimers.

Kinase Dimerization Increases Both Initial Velocity and Maximal Phosphate Incorporation of the Autophosphorylation. To evaluate the effect of kinase dimerization on the autophosphorylation reaction, we have performed time course experiments with both monomeric and dimeric kinases. The purified enzymes (0.5−1 μM) were autophosphorylated for 30 min in the presence of [γ^{32}P]ATP, and phosphate incorporation into the enzymes was determined after SDS−PAGE (see Experimental Procedures). As shown in Table 1 and Figure 4A and B, autophosphorylation of both monomeric kinases, IRKD and IGFKD, for 30 min resulted in phosphate incorporation of ∼2 mol/mol of kinase. In contrast, autophosphorylation of the dimeric kinases, GST-IRKD and GST-IGFK, resulted in incorporation of ∼4−4.5 mol of phosphate per mol of kinase subunit. Thus, maximal phosphate incorporation into the dimeric GST-tagged kinases was about 2-fold higher as compared to the monomeric nontagged kinases. Likewise, the initial velocities of the autophosphorylation for the dimeric GST-IGFKD and GST-IRKD were increased about 5−10-fold, as compared to the respective monomeric forms (Table 1; Figure 4A and B). As a result, the half-times for the autophosphorylation reaction were ∼40 s for both dimeric kinases, as compared to ∼3−5 min for the corresponding monomeric enzymes (Table 1; Figure 4A and B). Addition of equimolar amounts of purified GST to the kinase reaction of the monomeric IGFKD had no effect on the autophosphorylation of the enzyme (data not shown). Moreover, GST was not a substrate for any of the kinases in the present study (data not shown).

Kinase Dimerization Renders the Autophosphorylation Concentration-Independent. According to the kinetic analyses, the dimeric GST-tagged kinases show increased catalytic efficiencies in autophosphorylation reactions as compared to their monomeric counterparts. To address the question of whether the observed increase in the kinase activity is due to an increased efficiency of transphosphorylation of the dimeric enzymes, we have performed autophosphorylation reactions of the kinases in the absence of poly-L-lysine at two different enzyme concentrations. The results of these experiments are illustrated in Figure 4C. At a kinase concentration of 1 μM, autophosphorylation of the monomeric IRKD for 30 min resulted in a phosphate incorporation of 2 mol/mol, whereas the dimeric GST-IRKD incorporated 4−5 mol phosphate per mol of kinase subunit (Figure 4C). As shown in the figure, no significant change in the maximal phosphate incorporation was observed when the concentration of the dimeric GST-IRKD in the assay was increased to 15 μM. However, autophosphorylation of the monomeric IRKD at 15 μM for 30 min led to a phosphate incorporation of ∼4 mol/mol, almost identical to the phosphate incorporation of the dimeric enzyme (Figure 4C). Thus, consistent with recent reports (*13*, *14*), our data suggest that an increase in the local concentration of kinase molecules leads to an

Table 1: Kinetics of the Autophosphorylation of the Monomeric and Dimeric Kinases[a]

	maximal phosphate incorporation (mol/mol)		initial velocity (mol/(mol × min)		$t_{1/2}$ (sec)	
poly-L-lysine	−	+	−	+	−	+
IRKD	2.1 ± 0.2	4.7 ± 0.3	0.7 ± 0.2	7.2 ± 0.4	∼180	20 ± 3
GST-IRKD	4.4 ± 0.2	4.8 ± 0.6	3.5 ± 1.2	6.6 ± 1.1	43 ± 12	21 ± 4
IGFKD	1.2 ± 0.2	3.5 ± 0.8	0.2 ± 0.1	4.3 ± 0.4	∼300	27 ± 2
GST-IGFKD	3.4 ± 0.6	4.6 ± 1.5	2.5 ± 1.3	6.6 ± 2.4	40 ± 12	24 ± 2

[a] The kinases were phosphorylated in the presence (+) or absence (−) of equimolar amounts of poly-L-lysine as described in Experimental Procedures. Initial velocities were determined after 30 s of reaction time, and maximal phosphate incorporation was determined after 30 min of reaction time. Results are the means ±S.D. of at least two independent experiments performed in duplicates.

increased rate of transphosphorylation, resulting in a more efficient activation of the kinase.

Kinase Dimerization Eliminates the Stimulatory Effect of Poly-L-lysine on the Autophosphorylation. Previously, we (*11*) and others (*8*, *15*−*17*) have reported that addition of polycations (such as protamine and poly-L-lysine) to the phosphorylation reaction greatly enhances both the initial velocity of the enzyme and the maximal phosphate incorporation into the soluble insulin receptor kinase domain. It has been demonstrated that the effect of poly-L-lysine is due to a nonspecific kinase aggregation, presumably leading to a more efficient transphosphorylation of the kinases (*17*). Therefore, since the GST-tagged kinases are constitutive dimers, we expected a reduction in the poly-L-lysine-induced kinase activation as compared to that of the monomeric enzymes. To test this hypothesis, both the monomeric and dimeric kinases were autophosphorylated in time course experiments in the absence and presence of poly-L-lysine. As shown in Table 1 and Figure 5, stimulation of both monomeric kinases with poly-L-lysine resulted in a ∼10-fold increase in the initial velocities of the autophosphorylation reaction. Likewise, stimulation with poly-L-lysine led to a ∼2-fold increase in the maximal phosphate incorporation into the monomeric enzymes. In contrast, for both dimeric GST-kinases, stimulation with poly-L-lysine had little effect on the maximal phosphate incorporation as compared to the nonstimulated control.

Kinase Dimerization Increases the Catalytic Activity of the Kinases in Substrate Phosphorylation Reactions. Next, we have evaluated the catalytic activities of the monomeric and dimeric IRKDs in substrate phosphorylation reactions using the synthetic copolymer poly(Glu4:Tyr) (Table 2). As compared to that of the monomeric IRKD, the V_{max} value for the dimeric GST-IRKD was increased almost 20-fold (Table 2). On the other hand, the K_M values for poly(Glu_4:Tyr) for monomeric IRKD (75 μg/mL) and dimeric GST-IRKD (139 μg/mL) were comparable. As another, more physiological model substrate, we have employed a recombinant fragment derived from the human insulin receptor substrate-1 (IRS-1; ref *25*), the major cellular substrate of the insulin receptor. The 10 kDa IRS1-p10 contains two YMXM motifs that have been described as high affinity substrates for both the native human insulin receptor and the soluble insulin receptor kinase (*31*). As shown in Table 2, the maximum velocity of phosphoryl transfer was increased more than 100-fold for the dimeric GST-IRKD (11.5 mol min^{-1} per mol of kinase subunit) as compared to that of the monomeric IRKD (0.1 mol min^{-1} per mol of kinase). In contrast, the K_M values for the phosphorylation of IRS1-p10 were similar for both IRKD (K_M = 44.6 μM) and GST-

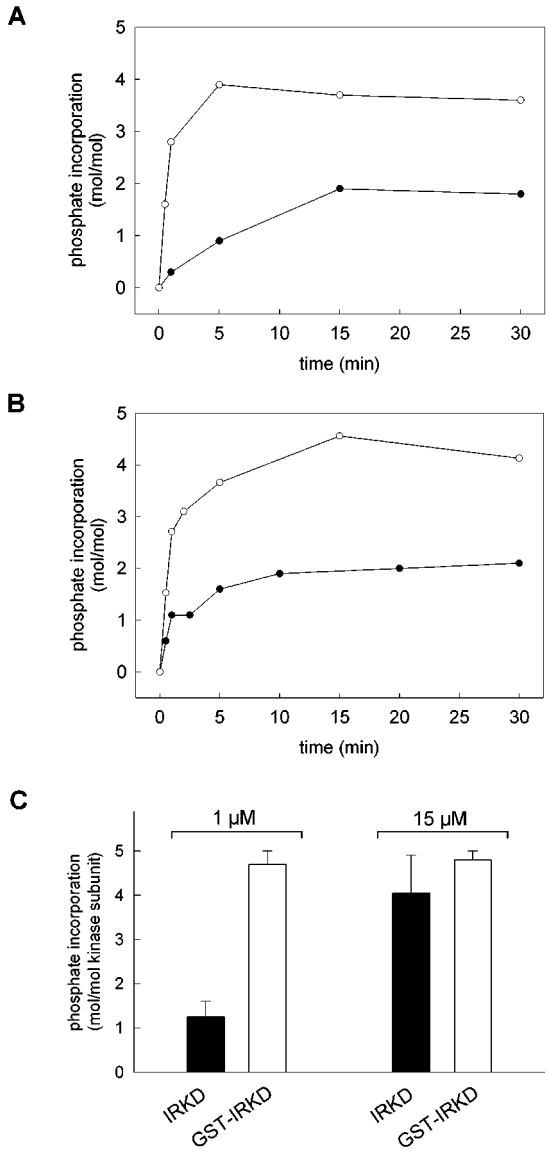

FIGURE 4: Dimerization enhances the autophosphorylation of the kinase and renders the autophosphorylation reaction concentration-independent. (A, B) The purified proteins were autophosphorylated at 0.5−1 μM in the presence of 250 μM [γ^{32}P]ATP for indicated times and resolved by SDS−PAGE. The incorporated radioactivity was determined by Cerenkov-counting of the excised bands (see Experimental Procedures). (A) Monomeric IRKD (closed circles, ●); dimeric GST-IRKD (open circles, ○). (B) Monomeric IGFKD (closed circles, ●); dimeric GST-IGFKD (open circles, ○). (C) Concentration-dependent autophosphorylation of monomeric IRKD and dimeric GST-IRKD. The purified kinases were autophosphorylated at indicated concentrations in the presence of 1 mM [γ^{32}P]-ATP for 30 min. After SDS−PAGE, the incorporated radioactivity was determined by Cerenkov-counting of the excised bands (see Experimental Procedures).

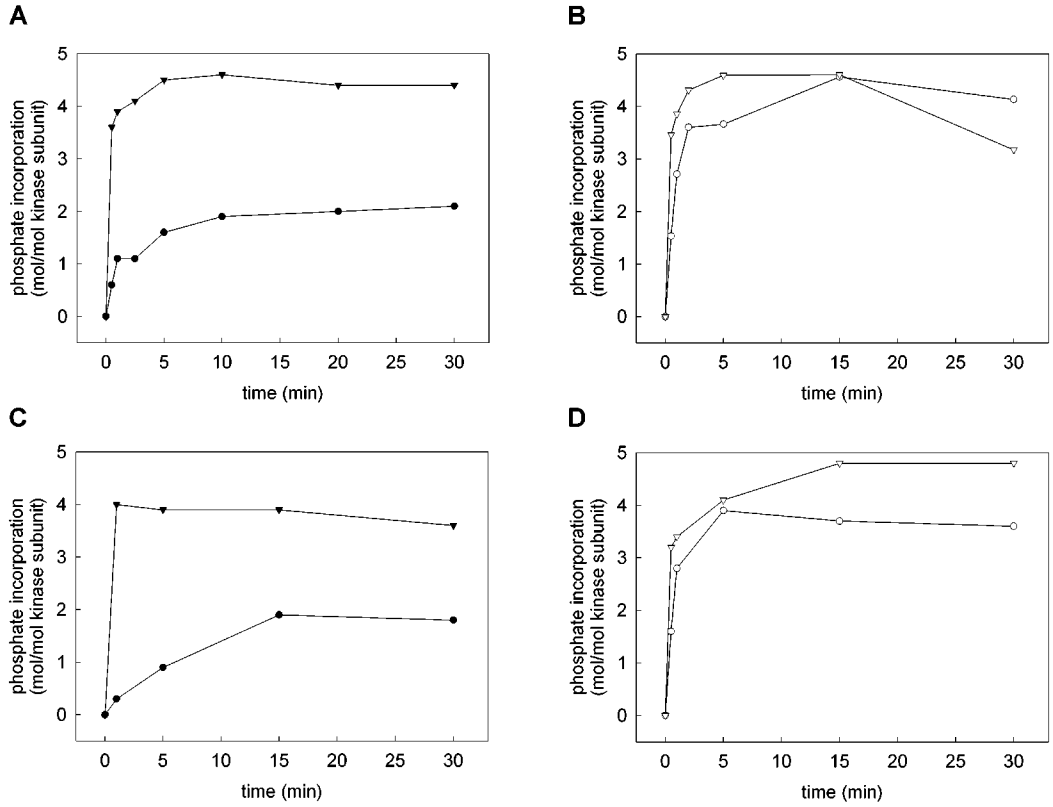

FIGURE 5: Dimerization eliminates the stimulatory effect of poly-L-lysine on the autophosphorylation reaction. The purified proteins were autophosphorylated at 0.5−1 μM in the absence (circles) and presence (triangles) of equimolar amounts of poly-L-lysine. Phosphate incorporation was determined by Cerenkov-counting of the excised bands (see Experimental Procedures). (A) IRKD; (B) GST-IRKD; (C) IGFKD; (D) GST-IGFKD.

Table 2: Dimerization Increases the Catalytic Activity of the Kinases in Substrate Phosphorylation Reactions[a]

	Glu_4:Tyr		IRS1-p10	
	K_M (μg/mL)	V_{max} (mol min^{-1} mol^{-1})	K_M (μM)	V_{max} (mol min^{-1} mol^{-1})
IRKD	75	3.6	44.6	0.1
GST-IRKD	139	67.4	52.9	11.5

[a] Substrate phosphorylation reactions using poly(Glu_4:Tyr) and IRS1-p10 were performed for 3 min as described in Experimental Procedures.

IRKD (K_M = 52.9 μM). In summary, depending on the substrate, the turnover number (k_{cat}) of the dimeric GST-IRKD is increased by 1 to 2 orders of magnitude as compared to that of the monomeric IRKD.

After Autophosphorylation, Kinase Dimerization Is Not Important for the Phosphorylation of Exogenous Substrates. Next, we have addressed the question of whether the dimeric structure of the autophosphorylated GST-IRKD is required for the observed increase in the catalytic activity of the enzyme toward exogenous substrates. In the experiment, the dimeric GST-IRKD was autophosphorylated in the presence of unlabeled ATP. The activated enzyme was then monomerized by thrombin cleavage of the GST tag. As judged by SDS−PAGE, the efficiency of thrombin cleavage of GST-IRKD exceeded 90% (data not shown). Finally, the kinases were diluted to 0.3 μM, and the phosphotransferase activity was assayed using poly(Glu4:Tyr). As illustrated in Figure 6, both the dimeric GST-IRKD and the monomerized IRKD showed comparable phosphotransferase activity toward poly-(Glu_4:Tyr), proving that dimerization of the kinase is not required for an efficient phosphorylation of exogenous substrates.

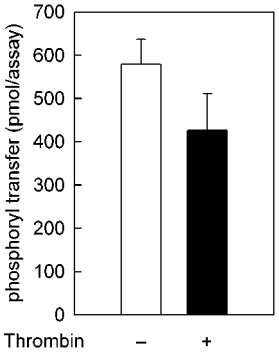

FIGURE 6: After autophosphorylation, kinase dimerization is not important for the phosphorylation of exogenous substrates. Substrate phosphorylation of activated GST-IRKD after proteolytic monomerization. Dimeric GST-IRKD (12 μM) was prephosphorylated at standard conditions for 10 min in the presence of unlabeled ATP, and the reaction was stopped by adding 15 mM EDTA. After incubation without (−) or with (+) thrombin (0.25 U) for 20 min, the kinase was diluted 40-fold in substrate phosphorylation reactions containing 0.7 mg/mL poly(Glu_4:Tyr) and 1 mM [γ^{32}P]ATP. After 12 min reaction time, phosphate incorporation into the substrate was determined as described in Experimental Procedures. The efficiency of thrombin cleavage of GST-IRKD was >90% as judged by SDS−PAGE (data not shown).

Kinase Dimerization Increases Bis- and Trisphosphorylation of the Activation Loop. To assess potential differences in the autophosphorylation of specific sites within the enzymes, we have characterized the autophosphorylation sites of the monomeric and dimeric insulin receptor kinases in

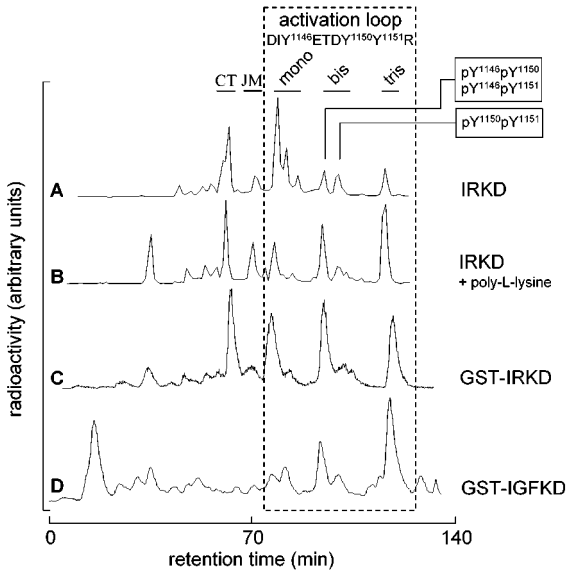

FIGURE 7: Kinase dimerization results in enhanced bis- and trisphosphorylation of the activation loop. Monomeric and dimeric kinases (1 μM) were autophosphorylated for 30 min in the presence of [γ^{32}P]ATP as described in Experimental Procedures. After SDS−PAGE, the radioactive bands were excised from the gel and digested with trypsin. The resulting phosphopeptides were separated and identified by HPLC anion exchange chromatography as described previously (*11*, *34*, *35*). CT, bis-phosphorylated C-terminal peptide of the IRKD/GST-IRKD: SpY^{1316}EEHIPpY^{1322}THMNGGK. mono-, bis-, and tris-, mono-, bis-, and trisphosphorylated forms of peptides derived from the activation loop of the IRKD/GST-IRKD/GST-IGFKD: DIpY^{1146}ETDpY^{1150}pY^{1151}R(KGGK). JM: juxtamembrane region of the IRKD/GST-IRKD containing pY^{960}.

the absence and presence of poly-L-lysine by HPLC-phosphopeptide mapping, respectively. The insulin receptor contains at least six potential tyrosine autophosphorylation sites: Y960 in the juxtamembrane region, Y1146, Y1150, and Y1151 in the activation loop, and Y1316 and Y1322 in the C-terminus of the enzyme (Figure 1). Similarly, IGFKD contains five homologous tyrosine autophosphorylation sites: Y950 in the juxtamembrane region, Y1131, Y1135, and Y1136 in the activation loop, and Y1316 in the C-terminus of the enzyme (Figure 1). After autophosphorylation, the kinases were subjected to SDS−PAGE, digested with trypsin, and the resulting [^{32}P]-labeled phosphopeptides were subjected to HPLC-anion exchange chromatography (see Experimental Procedures). Previously, we have identified the major peaks in the phosphopeptide profile of the IRKD by direct sequencing of the corresponding phosphopeptides and by analysis of phosphopeptide maps derived from IRKD mutants (*11*, *34*, *35*). As shown in Figure 7A, autophosphorylation of IRKD in the absence of poly-L-lysine resulted in the appearance of two major and several minor peaks. The two most prominent peaks corresponded to peptides containing the two C-terminal tyrosine phosphorylation sites, Y1316 and Y1322 (CT), and to the monophosphorylated form of the activation loop, containing tyrosine residues Y1146, Y1150, and Y1151. The minor peaks in the profile contained two different bisphosphorylated forms of the activation loop (pY1146/50 and/or pY1146/51; pY1150/51), the trisphosphorylated activation loop, and a phosphopeptide derived from the juxtamembrane region (JM; containing Y960). The phosphopeptide pattern of the monomeric IRKD phosphorylated in the presence of poly-L-lysine is shown in Figure 7B. In contrast to the nonstimulated kinase, the poly-L-lysine-activated enzyme showed two prominent peaks corresponding to the bis- (pY1146/50 and/or pY1146/51) and trisphosphorylated activation loop, respectively, whereas the peaks corresponding to the monophosphorylated activation loop were decreased. Notably, the peaks corresponding to the C-terminal phosphorylation sites and to the bisphosphorylated (pY1150/51) activation loop were unchanged as compared to the nonstimulated kinase.

The phosphopeptide map of the dimeric GST-IRKD phosphorylated in the absence of poly-L-lysine was almost identical to that of the poly-L-lysine-activated IRKD (Figure 7C). Moreover, the HPLC profile of GST-IRKD was not affected by the presence of poly-L-lysine in the autophosphorylation reaction (data not shown). As compared to that of the monomeric nonstimulated kinase, autophosphorylation of the activation loop in GST-IRKD was increased. However, whereas the bisphosphorylated forms of the activation loop, pY1146/50 and/or pY1146/51, were increased, the other bisphosphorylated form containing pY1150/51 was unchanged as compared to that of the monomeric enzyme (Figure 7A, C). Because of an identical amino acid sequence of the activation loops of IR and IGF-1R, the phosphopeptide pattern of GST-IGFKD was similar to that of GST-IRKD (Figure 7D). As for GST-IRKD, autophosphorylation of GST-IGFKD resulted in the appearance of mainly bis- (pY1131/35 and pY1131/36) and trisphosphorylated forms of the activation loop, whereas the mono and bis (pY1135/36) forms were represented as minor peaks in the map. Thus, dimerization leads to an increased transphosphorylation of the activation loop, resulting in an enhanced bis- (pY1146/50 and/or pY1146/51) and trisphosphorylation of the regulatory tyrosines.

Kinase Dimerization Does Not Occlude Binding Sites for p85-SH2 Domains. We next addressed the question of whether GST dimerization might affect the binding of potential signaling molecules to the kinase. Previously, it has been reported that the 85 kDa regulatory subunit of phosphatidylinositol (PI) 3-kinase (p85) binds directly via its SH2 domains to the C-terminal phosphotyrosines of the insulin receptor (*32*, *33*). However, the biological significance of this interaction remains to be clarified. Nevertheless, we have used an in vitro binding assay to monitor whether the binding sites required for this interaction are also accessible in the GST-dimerized IRKD. In the experiment, we used [^{32}P]-labeled GST-IRKD as a probe in Far-Western blots of immobilized recombinant p85-SH2 domains (see Experimental Procedures). As shown in Figure 8, GST-IRKD displayed a specific high affinity binding to the immobilized SH2 domain, indicating that the C-terminal phosphotyrosines required for this interaction are not occluded in the GST-dimerized enzyme.

Kinase Dimerization Leads to Conformational Changes in the Activation Loop. Limited proteolysis has been widely used to detect conformational changes in proteins (reviewed in ref *36*). To analyze whether dimerization of the IRKD results in a different conformation of the kinase, we have performed limited tryptic digests with both monomeric and dimeric kinases under various experimental conditions (see Experimental Procedures). As illustrated in Figure 9A, partial tryptic digest of the monomeric IRKD in the absence of adenine nucleotides resulted in the formation of a ~38 kDa

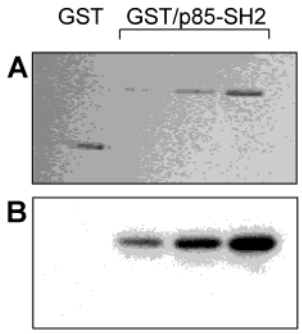

FIGURE 8: Kinase dimerization does not occlude binding sites for p85-SH2 domains. GST-p85-SH2 domain (1, 2.5, and 5 μg) and GST (10 μg) were applied to SDS−PAGE and transferred to a PVDF membrane. The membrane was then incubated with purified [^{32}P]-labeled GST-IRKD, washed, and exposed to a PhosphorImager screen (see Experimental Procedures). (A) Coomassie-stained SDS−PAGE. (B) Autoradiograph of bound [^{32}P]GST-IRKD.

trypsin-resistant fragment. As described previously (*12*, *37*), the ~38−41 kDa fragments are the cleavage product where trypsin cuts at two clusters of cleavage sites, R941, K942, and R943 in the N-terminus and K1271, R1292, and R1298 in the C-terminus of the IRKD, respectively (Figure 9D). In contrast, tryptic digest of the monomeric IRKD in the presence of 10 mM Mg^{2+}-ADP led to the appearance of an additional 24 kDa fragment (Figure 9A). This 24 kDa fragment is the result of trypsin cleavage of the IRKD 38 kDa trypsin-resistant fragment at a basic cluster (R1152, K1153, and K1156) in the activation loop of the IRKD (*37*) (Figure 9D). Thus, as demonstrated previously (*37*), adenine nucleotide binding of the monomeric IRKD causes a conformational change in the activation loop thereby enabling the protease to cleave the kinase at the activation loop. Consequently, the occurrence of the 24 kDa fragment indicates that the activation loop adopts a flexible, "gate open" conformation where the residues of the inhibitory activation loop are disengaged from the active site.

Surprisingly, for the dimeric kinase, generation of the 24 kDa fragment occurred independent of the presence of Mg^{2+}-ADP, indicating that the activation loop in the dimeric GST-IRKD constitutively adopts the open gate conformation (Figure 9A). In addition, tryptic digestion of GST-IRKD led to the appearance of a 27 kDa GST band that cross-reacted in Western Blots with an anti-GST antibody (Figure 9A, and data not shown). A more detailed analysis shows that tryptic digestion of GST-IRKD in the absence of nucleotides resulted in the concomitant appearance of both the GST band and the 24 kDa band, respectively (Figure 9B). However, no increase in activation loop cleavage was observed after the GST tag was completely removed, indicating that the activation loop becomes inaccessible to trypsin when the kinase is monomerized in the absence of ADP (Figure 9B). The identity of the 24 kDa fragment was confirmed by tryptic digestion of the [^{32}P]-labeled kinases (Figure 9C) and by HPLC phosphopeptide mapping of the excised band (data not shown). Thus, whereas Mg^{2+}-ADP binding or autophosphorylation of the monomeric kinase is required for trypsin cleavage of the activation loop, cleavage of the dimeric kinase at the activation loop is not restricted to prior autophosphorylation or adenine nucleotide binding (Figure 9A and B).

DISCUSSION

The contribution of the dimeric structure of the insulin receptor (IR)/insulin-like growth factor receptor (IGF-1R) to the function of the kinase is not well understood. To address this issue, we have constructed soluble monomeric and dimeric kinase domains derived from the IR and IGF-1R, respectively. While both receptors, IR and IGF-1R, have different biological profiles in vivo (*38*), the soluble kinases behave very similar in vitro, due to the high sequence homology in their kinase domains (>80% identity, >90% similarity). As a dimerization module for the kinases, we have chosen glutathione *S*-transferase from *Schistosoma japonicum*. The homodimeric structure of GST provides both an affinity tag for purifying the recombinant proteins and a powerful tool in studying protein−protein interactions (*22*, *23*, *26*). Although the GST−GST interaction does not involve disulfide bonds, the dimers are highly stable and only dissociate under denaturating conditions, such as treatment with 6 M urea (*39*). The monomeric and dimeric GST-tagged receptor kinases used in the present study were expressed in insect cells via the baculovirus system and purified to homogeneity in mg quantities.

The homodimeric nature of the GST-receptor kinase fusion proteins was confirmed by native gradient gel electrophoresis and MALDI-TOF mass spectroscopy (Figure 3). Kinetic analyses of autophosphorylation reactions using the monomeric and dimeric kinases revealed that the latter enzymes displayed a greatly enhanced catalytic activity (Figures 4 and 5; Tables 1 and 2). The initial velocities of the autophosphorylation reaction for the dimeric kinases were increased up to 10-fold, as compared to the corresponding monomeric forms. Moreover, as compared to the monomeric kinases, stimulation of the dimeric GST-kinases with poly-L-lysine had little effect on both initial velocity and maximal phosphate incorporation in the autophosphorylation reaction. On the contrary, even at submicromolar kinase concentrations, the kinetics of phosphoryl transfer observed with the dimeric GST-kinase were almost identical to the kinetics of the monomeric enzyme in the presence of poly-L-lysine, suggesting that the stimulatory effect of the polycation is mainly due to the cross-linking of the kinases (Figure 5). Thus, GST-mediated dimerization of the kinases results in a very rapid ($t_{1/2} \approx 0.5$ min) autoactivation of the kinases, independent of the kinase concentration and the artificial stimulation with polycations. Indicative of the high intrinsic activity of the dimeric kinases, the maximum velocities (V_{max}) of phosphoryl transfer toward two different substrates, poly-(Glu_4:Tyr) and IRS1-p10, were increased 20-fold and 100-fold, respectively, whereas the corresponding K_M values were almost unchanged as compared to the monomeric kinase controls (Table 2). Furthermore, once the dimeric kinase has been autophosphorylated, it remains fully active even at low concentrations after subsequent monomerization of the protein by proteolytic removal of the GST tag (Figure 6). These findings demonstrate that dimerization is essential for the observed rapid autophosphorylation but not for the enhanced kinase activity in substrate phosphorylation reactions.

At low to moderate enzyme concentrations (~1 μM) in the absence of poly-L-lysine, autophosphorylation of both monomeric kinases, IRKD and IGFKD, resulted in phosphate

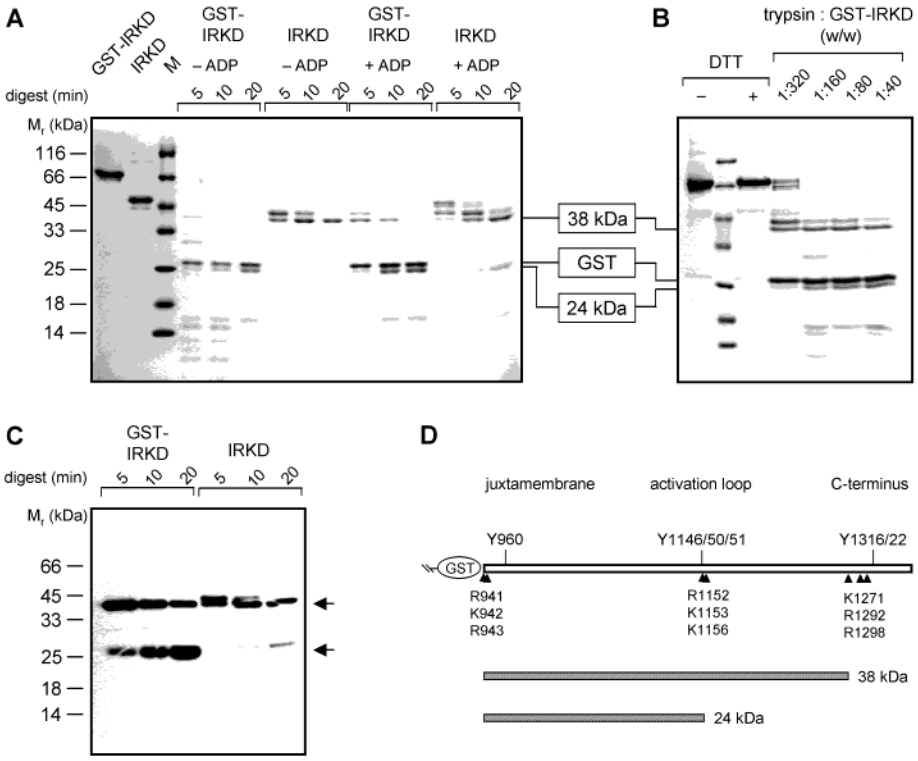

FIGURE 9: Kinase dimerization leads to changes in the conformation of the activation loop. (A) For limited proteolysis of monomeric IRKD and dimeric GST-IRKD, the enzymes were incubated with trypsin (1:80 w/w) for indicated times in the absence and presence of Mg^{2+}-ADP as described in Experimental Procedures, and the samples were then separated by 15% SDS−PAGE and Coomassie-stained. (B) GST-IRKD was incubated with indicated amounts of trypsin for 4 min, separated by 15% SDS−PAGE, and Coomassie-stained. Purified GST-IRKD was analyzed under nonreducing (−) and reducing (+) conditions (DTT, dithiothreitol, 100 mM). (C) Autoradiograph of the partially digested [^{32}P]-labeled kinases. IRKD and GST-IRKD were incubated in the presence of Mg^{2+}-[γ^{32}P]ATP for 30 min as described in Experimental Procedures. The samples were then incubated with trypsin (1:80 w/w) for indicated times. After separation by 15% SDS−PAGE, the gel was exposed to an X-ray film. The phosphorylated 24 kDa fragment showed an apparent mobility shift to 27 kDa. Arrows indicate the positions of the 38 kDa fragment and the shifted 24 kDa fragment. (D) Schematic representation of the main tryptic cleavage sites of GST-IRKD. Also indicated are the three subdomains of the soluble kinase and the positions of the tyrosine autophosphorylation sites.

incorporation of only ~2 mol/mol of enzyme, whereas under the same assay conditions, maximum phosphate incorporation for both dimeric kinases was ~4−5 mol/mol of kinase subunit (Figures 4 and 5; Table 1), indicating that under these conditions, autophosphorylation of the monomeric kinase results only in partial phosphorylation of the activation loop, failing to fully activate the enzyme. Indeed, according to the HPLC-phosphopeptide maps, the monomeric kinases phosphorylated at low concentration (1 μM) in the absence of poly-L-lysine show mainly monophosphorylated forms of the activation loop (Figure 7A), consistent with the low intrinsic activity of the enzymes. In contrast, phosphorylation of the activation loop in the GST-tagged kinase as well as in the poly-L-lysine-activated IRKD was shifted to the bis- and trisphosphorylated forms (Figure 7B−D). These data suggest that bis- and trisphosphorylation of the catalytic loop are mediated by transphosphorylation, whereas the monophosphorylation of the activation loop occurs in cis. However, it should be noted that because of potentially different recoveries of individual peptides in the HPLC analyses, the integrated radioactivity of a certain peak does not allow the exact determination of the absolute amount of phosphorylation of the corresponding site.

The crystal structure of the phosphorylated monomeric IRKD provides evidence that autophosphorylation of the three regulatory tyrosines, Y1146, Y1150, and Y1151, stabilizes a conformation of the activation loop in which the active site is accessible to metal-ATP and peptide substrate (*41*, *42*). In contrast, in the nonphosphorylated IRKD, the activation loop obstructs the active site of the enzyme and prevents access of metal-ATP to the ATP binding site (*40*−*42*). It has been proposed that transphosphorylation of Y1150 causes a relief of this inhibition by stabilizing the activation loop in a conformation that allows metal-ATP binding. Subsequently, these events should lead to further phosphorylation of tyrosines in the activation loop and, as a result, to full activation of the kinase (*12*). This model is in line with biochemical data that indicate that at least bisphosphorylation of the activation loop is sufficient for maximum kinase activity (*12*). Several studies have analyzed the course of phosphorylation of the activation loop in the insulin receptor kinase, but all came to different conclusions (*10*, *12*, *43*−*45*). Whereas transphosphorylation of Y1150 was considered as an early event in the autophosphorylation of a truncated monomeric IRKD (*12*), previous studies with the native insulin receptor concluded that phosphorylation of Y1146 is a key step in receptor autophosphorylation. Yet, in another monomeric IRKD construct, Y1146 was the least phosphorylated, and bisphosphorylation of the activation loop occurred mainly at Y1150/51 (*10*). In contrast, in the native insulin receptor, the predominant bisphosphorylated form of the activation loop was found to contain pY1146 and either pY1150 or pY1151 (*43*−*45*). Consistent with the latter report, our data demonstrate that activation of the kinase by

either GST fusion or addition of poly-L-lysine to the monomeric kinase was accompanied by the occurrence of a bisphosphorylated peptide containing pY1146 (pY1146/50 and/or pY1146/51; Figure 7). In contrast, the bisphosphorylated activation loop containing pY1150/51 was always found to be a minor form and clearly does not correlate with the kinase activity. Since significant phosphorylation of Y1146 in the bisphosphorylated activation loop of the IRKD was only detectable in the GST-dimerized or polycation-oligomerized kinase, respectively (Figure 7), we propose a transphosphorylation mechanism for Y1146. This mechanism might explain the observed predominance of Y1146 phosphorylation in the dimeric insulin holoreceptor. Interestingly, of all the three phosphotyrosines in the activation loop, pY1146 has been shown to be the primary target of the human tyrosine phosphatase LAR (*46*). Although in a previous study we were unable to detect a major impact of the Y1146 → F mutation on the kinase activity of a monomeric IRKD mutant (*34*), it has been shown for the dimeric insulin receptor that mutation of Y1146 to phenylalanine renders the receptor biologically inactive (*47*), implicating a possible regulatory role of Y1146 in the insulin receptor signaling. Thus, it would be interesting to study the effect of this mutation in a GST-kinase dimer.

Whereas the crystal structure of the nonphosphorylated monomeric IRKD clearly shows that the activation loop serves as an intrasteric inhibitor of the ATP-binding region, it has been reported recently that in solution the nonphosphorylated activation loop in the IRKD is partially disengaged from the active site ("open gate" conformation) at physiological ATP concentrations (*37*). Hence, the evidence for a regulatory role of adenine nucleotide binding to the kinase in vivo remains to be established. Nevertheless, the observed differences in the phosphorylation pattern of the regulatory activation loop in the monomeric versus dimeric kinases suggested that in the dimeric kinase, the activation loop adopts an altered conformation as compared to that of the monomeric kinase. To test whether GST-induced dimerization by itself causes a restructuring of the activation loop, we have used limited proteolysis to probe its conformation (Figure 9). As described previously for the IRKD, tryptic cleavage of the activation loop only occurs when the enzyme is in its adenine nucleotide bound form (*37*), where the activation loop is disengaged from the active site and exposed to the solvent ("gate open", i.e., active conformation). Furthermore, we show that tryptic cleavage of the activation loop occurs when the enzyme has been autophosphorylated (Figure 9C). As a result, tryptic digestion of the kinase generates a 24 kDa fragment corresponding to basic residues around R941 in the N-terminus of the kinase and around R1152 in the activation loop (Figure 9D and ref *37*). Surprisingly, tryptic cleavage of the activation loop of GST-IRKD takes place independent of nucleotide binding (Figure 9A and B), demonstrating that in the dimeric kinase the activation loop is locked in the "gate open" conformation even in the absence of bound nucleotides.

Noticeably, the removal of the GST tag occurs very rapidly; within less than 5 min, the GST tag was completely cleaved off from the kinase (Figure 9A), leading to the appearance of the 27 kDa GST band and the 24 kDa kinase fragment. Since removal of the GST tag leads to a monomerization of the kinase, an ongoing activation loop cleavage is only observed in the presence of nucleotides. In the presence of ADP, the activation loop of the kinase is accessible to trypsin cleavage regardless of the monomeric or dimeric state of the enzyme (Figure 9A and ref *37*). Consequently, activation loop cleavage (i.e., production of the 24 kDa band) is observed even after complete removal of the dimerizing GST tag (see Figure 9A, 5 min versus 10 min time points). In contrast, in the absence of nucleotides, trypsin cleavage of GST-IRKD occurs simultaneously in the juxtamembrane region and in the activation loop of the kinase, resulting in the concurrent appearance of both the GST-band and the 24 kDa fragment. Most importantly, no increase in activation loop cleavage was observed after the GST tag was completely removed, indicating that the activation loop becomes inaccessible to trypsin when the kinase is monomerized in the absence of ADP (Figure 9B). Consistent with a monomerization of the kinase after GST cleavage, we did not find any evidence for dimerization of the kinases via disulfide bonds (Figure 9B). Thus, GST-mediated dimerization by itself has a major impact on the structure of the kinase by stabilizing the activation loop in a conformation that corresponds to the active form of the kinase.

Even though GST dimerization leads to an increased kinase activity of the enzyme, dimerization of the insulin receptor β subunits by substitution of the transmembrane domains with those of glycophorin A failed to activate the receptor kinase (*21*). This is in contrast to other examples where activation of a protein kinase was induced by fusion to a heterologous dimerization domain (*48*, *49*), including fusion to GST (*50*). These findings suggest that dimerization of tyrosine kinases is not by itself sufficient for kinase activation but rather requires a distinct spatial conformation of the kinase molecules (*19*). According to the model of Yip et al. (*4*, *5*) that has been developed from three-dimensional reconstruction of the insulin-ligated insulin receptor, insulin binding to the receptor causes a spatial rearrangement of the two kinase subunits, thereby allowing the activation loop of one kinase subunit to reach the active site of the other kinase subunit. Obviously, the positioning of the two kinase domains within the GST dimer similarly fulfills the spatial requirement for an efficient trans-activation of the enzyme.

Because both poly-L-lysine-mediated oligomerization of the monomers and GST-mediated dimerization of the kinase result in the very same autophosphorylation pattern of the activation loop, one might speculate that the monomeric kinases have an intrinsic tendency to self-interact. The kinetics of the limited proteolysis clearly show that the dimeric GST-IRKD is more rapidly degraded than the corresponding monomeric form, indicating an increased flexibility within the molecules in the dimeric state (Figure 9A). Thus, dimerization of the IRKD via GST perhaps does not introduce a rigid clamp but rather permits a certain flexibility within the dimer that may be required for the two kinase domains to productively align themselves to another.

In summary, the dimeric GST-kinases are primed to rapid autoactivation. GST-mediated dimerization by itself causes a conformational change in the activation loop that has been shown previously to resemble the active conformation of the enzyme. Therefore, dimerization-induced activation of the kinases provides an alternative mechanism to the proposed "cis-inhibition/trans-activation" model (*6*). In addition, dimer-

ization greatly increases the local concentration of both phosphoryl donor and phosphoryl acceptor sites, respectively. As a consequence, transphosphorylation of key residues within the activation loops between kinase subunits is kinetically preferred. Thus, it is tempting to speculate that the GST-kinases resemble the spatial arrangement of the two kinase subunits in the corresponding hormone-bound holoreceptor complex as proposed by Yip and co-workers (*4*, *5*). Since the GST-dimerized kinases share several features of the corresponding native receptors, they apparently present a useful model system for further studies that may help to understand the molecular mechanism that is responsible for the ligand-induced activation of the insulin receptor-like holoreceptors.

ACKNOWLEDGMENT

We greatly acknowledge Dr. Reinhard Sterner for helpful discussions and for critically reading the manuscript. We also thank Dr. Franz-Josef Marner for the MALDI analyses, Dr. Dirk Müller-Wieland for kindly providing the IRS-1 cDNA, and Sabine Lohmer and Monika Gompert for expert technical assistance.

REFERENCES

1. Ullrich, A., and Schlessinger, J. (1990) *Cell 61*, 203−212.
2. Flörke, R. R., Klein, H. W., and Reinauer, H. (1990) *Eur. J. Biochem. 191*, 473−482.
3. Heldin, C.-H. (1995) *Cell 80*, 213−223.
4. Luo, R. Z.-T., Beniac, D. R., Fernandes, A. B., Yip, C. C., and Ottensmeyer, F. P. (1999) *Science 285*, 1077−1080.
5. Ottensmeyer, F. P., Beniac, D. R., Luo, R. Z., and Yip, C. C. (2000) *Biochemistry 39*, 12103−12112.
6. Hubbard, S. R., Mohammadi, M., and Schlessinger, J. (1998) *J. Biol. Chem. 273*, 11987−11990.
7. Villalba, M., Wente, S. R., Russell, D. S., Ahn, J., Reichelderfer, C. F., and Rosen, O. M. (1989) *Proc. Natl. Acad. Sci. U.S.A. 89*, 7848−7852.
8. Cobb, M. H., Sang, B.-C., Gonzales, R., Goldsmith, E., and Ellis, L. (1989) *J. Biol. Chem. 264*, 18701−18706.
9. Kohanski, R. A. (1993) *Biochemistry 32*, 5766−5772.
10. Kohanski, R. A. (1993) *Biochemistry 32*, 5773−5780.
11. Al-Hasani, H., Eisermann, B., Tennagels, N., Magg, C., Passlack, W., Koenen, M., Müller-Wieland, D., Meyer, H. E., and Klein, H. W. (1997) *FEBS Lett. 400*, 65−70.
12. Wei, L., Hubbard, S. R., Hendrickson, W. A., and Ellis, L. (1995) *J. Biol. Chem. 270*, 8122−8130.
13. Bishop, S. M., Ross, J. B. A., and Kohanski, R. A. (1999) *Biochemistry 38*, 3079−3089.
14. Ablooglu, A. J., Till, J. H., Kim, K., Parang, K., Cole, P. A., Hubbard, S. R., and Kohanski, R. A. (2000) *J. Biol. Chem. 275*, 30394−30398.
15. Rosen, O. M., and Lebwohl, D. E. (1988) *FEBS Lett. 231*, 397−401.
16. Fujita-Yamaguchi, Y., Sacks, D. B., McDonald, J. M., Sahal, D., and Kathuria, S. (1989) *Biochem. J. 263*, 813−822.
17. Kohanski, R. A. (1989) *J. Biol. Chem. 264*, 20984−20991.
18. Lee, J., Shoelson, S. E., and Pilch, P. F. (1995) *J. Biol. Chem. 270*, 31136−31140.
19. Hunter, T. (1999) *Curr Biol. 9*, R568−571.
20. Burke, C. L., Lemmon, M. A., Coren, B. A., Engelman, D. M., and Stern, D. F. (1997) *Oncogene 14*, 687−696.
21. Gardin, A., Auzan, C., Clauser, E., Malherbe, T., Aunis, D., Cremel, G., and Hubert, P. (1999) *FASEB J. 13*, 1347−1357.
22. Parker, M. W., Lo Bello, M., Federici, G. (1990) *J. Mol. Biol. 213*, 221−222.
23. Ji, X., Zhang, P., Armstrong, R. N., and Gilliland, G. L. (1992) *Biochemistry 31*, 10169−10184.
24. Tennagels, N., Hube-Magg, C., Wirth, A., Noelle, V., and Klein, H. W. (1999) *Biochem. Biophys. Res. Commun. 260*, 724−728.
25. Sun, X. J., Rothenberg, P., Kahn, C. R., Backer, J. M., Araki, E., Wilden, P. A., Cahill, D. A., Goldstein, B. J., and White, M. F. (1991) *Nature 352*, 73−77.
26. Smith, D. B., and Johnson, K. S. (1988) *Gene 67*, 31−40.
27. Sahal, D., and Fujita-Yamaguchi, Y. (1987) *Anal. Biochem. 167*, 23−30.
28. Laemmli, U. K. (1970) *Nature 227*, 680−685.
29. Blakesley, R. W., and Boezi, J. A. (1977) *Anal. Biochem. 82*, 580−582.
30. Bradford, M. M. (1976) *Anal. Biochem. 72*, 248−254.
31. Siemeister, G., Al-Hasani, H., Klein, H. W., Kellner, S., Streicher, R., Krone, W., and Müller-Wieland, D. (1995) *J. Biol. Chem. 270*, 4870−4874.
32. Sanchez-Margalet, V., Goldfine, I. D., Truitt, K., Imboden, J., and Sung, C. K. (1995) *Mol. Endocrinol. 9*, 435−442.
33. Staubs, P. A., Reichart, D. R., Saltiel, A. R., Milarski, K. L., Maegawa, H., Berhanu, P., Olefsky, J. M., and Seely, B. L. (1994) *J. Biol. Chem. 269*, 27186−27192.
34. Noelle, V., Tennagels, N., and Klein, H. W. (2000) *Biochemistry 39*, 7170−7177.
35. Tennagels, N., Bergschneider, E., Al-Hasani, H., and Klein, H. W. (2000) *FEBS Lett. 479*, 67−71.
36. Hubbard, S. J. (1998) *Biochim. Biophys. Acta 1382*, 191−206.
37. Frankel, M., Bishop, S. M., Ablooglu, A. J., Han, Y. P., and Kohanski, R. A. (1999) *Protein Sci. 8*, 2158−2165.
38. Blakesley, V. A., Scrimgeour, A., Esposito, D., and Le Roith, D. (1996) *Cytokine Growth Factor Rev. 7*, 153−159.
39. Hornby, J. A., Luo, J. K., Stevens, J. M., Wallace, L. A., Kaplan, W., Armstrong, R. N., and Dirr, H. W. (2000) *Biochemistry 39*, 12336−12344.
40. Hubbard, S. R., Wei, L., Ellis, L., and Hendrickson, W. A. (1994) *Nature 372*, 746−754.
41. Hubbard, S. R. (1997) *EMBO J. 16*, 5572−5581.
42. Hubbard, S. R. (1999) *Prog. Biophys. Mol. Biol. 71*, 343−358.
43. White, M. F., Shoelson, S. E., Keutmann, H., and Kahn, C. R. (1988) *J. Biol. Chem. 263*, 2969−2980.
44. Flores-Riveros, J. R., Sibley, E., Kastelic, T., and Lane, M. D. (1989) *J. Biol. Chem. 264*, 21557−21572.
45. Tavaré, J. M., and Denton, R. M. (1988) *Biochem. J. 252*, 607−615.
46. Lee, J. P., Cho, H., Bannwarth, W., Kitas, E. A., and Walsh, C. T. (1992) *Protein Sci. 1*, 1353−1362.
47. Wilden, P. A., Backer, J. M., Kahn, C. R., Cahill, D. A., Schroeder, G. J., and White, M. F. (1990) *Proc. Natl. Acad. Sci. U.S.A. 87*, 3358−3362.
48. Farrar, M. A., Alberola-Ila, J., and Perlmutter, R. M. (1996) *Nature 383*, 178−181.
49. Luo, Z., Tzivion, G., Belshaw, P. J., Vavvas, D., Marshall, M., and Avruch, J. (1996) *Nature 383*, 181−185.
50. Maru, Y., Afar, D. E., Witte, O. N., and Shibuya, M. (1996) *J. Biol. Chem. 271*, 15353−15357.

BI015588G